

# Measurement of the jet width in $\gamma\gamma$ collisions and in $e^+e^-$ annihilation process at TRISTAN \*

TOPAZ Collaboration

## Abstract

The shape of jets produced in (quasi-) real photon-photon collisions as well as in  $e^+e^-$  annihilation process has been studied with a cone jet finding algorithm, using the data taken with the TOPAZ detector at the TRISTAN  $e^+e^-$  collider at an average center-of-mass energy ( $\sqrt{s_{ee}}$ ) of 58 GeV. The results are presented in terms of the jet width as a function of the jet transverse energy ( $E_T^{jet}$ ) as well as a scaled transverse jet energy,  $x_T$  ( $=2 \cdot E_T^{jet} / \sqrt{s}$ ). The jet width narrows as  $E_T^{jet}$  increases; however, at the same value of  $E_T^{jet}$  the jet width in  $\gamma\gamma$  collisions at TRISTAN is significantly narrower than that in  $\gamma p$  collisions at HERA. By comparing our results with the data in other reactions, it has been shown that the jet width in  $\gamma\gamma$ ,  $\gamma p$ ,  $p\bar{p}$  collisions as well as the  $e^+e^-$  annihilation process has an approximate scaling behavior as a function of  $x_T$ .

---

\*To be published in Phys. Lett. **B**.

# The TOPAZ Collaboration

K.Adachi<sup>(1)</sup>, H. Hayashii<sup>(1)†</sup>, K. Miyabayashi<sup>(1)</sup>, S. Noguchi<sup>(1)</sup>, A. Miyamoto<sup>(2)</sup>,  
T. Tauchi<sup>(2)</sup>, K. Abe<sup>(3)</sup>, T. Abe<sup>(3)‡</sup>, I. Adachi<sup>(2)</sup>, M. Aoki<sup>(3)</sup>, M. Aoki<sup>(4)</sup>, R. Enomoto<sup>(2)</sup>,  
K.Emi<sup>(2)</sup>, H. Fujii<sup>(2)</sup>, K. Fujii<sup>(2)</sup>, T. Fujii<sup>(6),(10)</sup>, J. Fujimoto<sup>(2)</sup>, N. Fujiwara<sup>(1)</sup>, H. Hirano<sup>(5)</sup>,  
B. Howell<sup>(8)</sup>, N. Iida<sup>(2)</sup>, H. Ikeda<sup>(2)</sup>, Y. Inoue<sup>(7)</sup>, S. Itami<sup>(3)</sup>, R. Itoh<sup>(2)</sup>, H. Iwasaki<sup>(2)</sup>,  
M. Iwasaki<sup>(1)§</sup>, R. Kajikawa<sup>(3)</sup>, K. Kaneyuki<sup>(4)</sup>, S. Kato<sup>(9)</sup>, S. Kawabata<sup>(2)</sup>, H. Kichimi<sup>(2)</sup>,  
M. Kobayashi<sup>(2)</sup>, D. Koltick<sup>(8)</sup>, I. Levine<sup>(8)</sup>, H. Mamada<sup>(5)</sup>, K. Muramatsu<sup>(1)</sup>, K. Nagai<sup>(10)¶</sup>,  
K. Nakabayashi<sup>(3)</sup>, M. Nakamura<sup>(7)</sup>, E. Nakano<sup>(7)</sup>, O. Nitoh<sup>(5)</sup>, A. Ochi<sup>(4)</sup>, F. Ochiai<sup>(11)</sup>,  
N. Ohishi<sup>(3)</sup>, Y. Ohnishi<sup>(2)</sup>, Y. Ohshima<sup>(4)</sup>, H. Okuno<sup>(2)</sup>, T. Okusawa<sup>(7)</sup>, E. Shibata<sup>(8)</sup>,  
A. Sugiyama<sup>(3)</sup>, H. Sugiyama<sup>(1)</sup>, S. Suzuki<sup>(3)</sup>, K. Takahashi<sup>(5)</sup>, T. Takahashi<sup>(7)</sup>,  
T. Tanimori<sup>(4)</sup>, Y. Teramoto<sup>(7)</sup>, M. Tomoto<sup>(3)</sup>, T. Tsukamoto<sup>(2)</sup>, T. Tsumura<sup>(5)</sup>, S. Uno<sup>(2)</sup>,  
Y. Watanabe<sup>(4)</sup>, A. Yamamoto<sup>(2)</sup>, and M. Yamauchi<sup>(2)</sup>

<sup>(1)</sup>*Department of Physics, Nara Women's University, Nara 630-8506, Japan*

<sup>(2)</sup>*KEK, High Energy Accelerator Research Organization, Tsukuba, Ibaraki 305-0801, Japan*

<sup>(3)</sup>*Department of Physics, Nagoya University, Nagoya 464-8601, Japan*

<sup>(4)</sup>*Department of Physics, Tokyo Institute of Technology, Tokyo 152-8551, Japan*

<sup>(5)</sup>*Dept. of Applied Physics, Tokyo Univ. of Agriculture and Technology, Tokyo 184-8588,  
Japan*

<sup>(6)</sup>*Department of Physics, University of Tokyo, Tokyo 113-0033, Japan*

<sup>(7)</sup>*Department of Physics, Osaka City University, Osaka 558-8585, Japan*

<sup>(8)</sup>*Department of Physics, Purdue University, West Lafayette, IN 47907, USA*

<sup>(9)</sup>*Institute for Nuclear Study, University of Tokyo, Tokyo 188-0002, Japan*

<sup>(10)</sup>*The Graduate School of Science and Technology, Kobe University, Kobe 657-8501, Japan*

<sup>(11)</sup>*Faculty of Liberal Arts, Tezukayama Gakuin University, Nara 631, Japan*

---

<sup>†</sup>e-mail address: hayashii@hepl.phys.nara-wu.ac.jp

<sup>‡</sup>Present address: Stanford Linear Accelerator Center, Stanford University, Stanford, California 94309, USA

<sup>§</sup>Present address: University of Oregon, Eugene, OR 97403, USA

<sup>¶</sup>Present address: EP division, CERN, CH-1211, Geneva 23, Switzerland

# 1 Introduction

At  $e^+e^-$  colliders copious photons are emitted from the beam electrons or positrons, where most of the photons carry only a small four-momentum squared ( $Q^2$ ), and can be considered to be quasi-real ( $Q^2 \approx 0$ ). These quasi-real photons can interact with each other and produce hadrons in the final state. Before TRISTAN experiments, hadron production in quasi-real photon-photon ( $\gamma\gamma$ ) collisions had generally been thought to be mainly caused by soft processes, and that perturbative-QCD can not be applied. This situations drastically changed when the production of high-transverse-energy ( $E_T^{jet}$ ) jets was observed in  $\gamma\gamma$  interactions at TRISTAN[1, 2] and LEP[3]  $e^+e^-$  colliders.

High- $E_T^{jet}$  jet production in  $\gamma\gamma$  collisions is an interesting field to study the photon structure and to test perturbative QCD predictions. Since the photon can fluctuate into hadronic components before interactions, three classes of hard QCD processes are expected to contribute to jet production at the leading order (LO)[4, 5]: either as a direct process where two photons directly interact (Fig.1a), one-resolved process where a bare photon interacts with a parton (quark or gluon) of the other photon (Fig.1b), or a two-resolved process where partons of both photons interact (Fig.1c). The jet cross sections as a function of  $E_T^{jet}$  were measured up to 8 GeV by TOPAZ[1] and AMY[2], and were compared with the next-leading-order QCD calculations in refs.[6] and [7]. Recently, the jet cross sections were measured up to 17 GeV at LEP2 by OPAL[8]. The existence of the remnant-jet, i.e. accompanied hadronic activities in the low-angle region, is a direct signature of the resolved processes. This signature has been observed in TOPAZ[1, 9] and OPAL[8] experiments. It has been reported that the charm-quark production in  $\gamma\gamma$  collisions requires the resolved-photon processes[10]. The necessity of gluon contents in the photon is emphasized in ref.[1, 10]. In photon-hadron interactions, similar QCD predictions have already been confirmed at the HERA  $ep$  collider[11, 12].

In addition to production rates of jets, the internal structure of jets, i.e. jet shape or jet profile, is expected to provide additional information about the QCD dynamics [13]-[16]. The shape might depend on the type of primary parton; quark or gluon. However, it also depends on the kinematical variables, such as the transverse energy and rapidity of the jets, as well as the jet algorithm. Theoretically, the jet shape is related to the ratio of the higher-order cross sections divided by the leading-order cross sections[14, 16]. Therefore, the next-leading-order (NLO) calculation of the jet rates provides leading-order predictions on the jet shape[16]. Although NLO predictions on the jet shape in hadron (or photon) interactions are not yet available, it is suggested in ref.[14] that the jets in hadron-hadron, photon-hadron and photon-photon collisions at different c.m. energies ( $\sqrt{s}$ ) should have the same shape for an equal value of the scaled variable  $x_T = \frac{2E_T^{jet}}{\sqrt{s}}$  at the fixed value of the jet pseudorapidity( $\eta^{jet}$ )<sup>||</sup>. A small deviation from the scaling behavior is expected only through

---

<sup>||</sup>This expectation is based on the following arguments[14]. The  $E_T^{jet}$  dependence in the jet shape is mainly caused by the dependence in the hard sub-process cross sections. However, the sub-process cross sections depend only on dimensionless variables,  $x_T$ ,  $\eta$  and the momentum fraction  $x_{a,b}$  of the incoming partons and other dimensional factors cancel in the ratio. Since  $x_{a,b}$  have been integrated over in the observable, the jet shape depends only on  $x_T$  for fixed  $\eta^{jet}$ . In the experiments, the jet shape in the central region ( $|\eta^{jet}| < 1.0$ ) has been mainly measured so far.

the  $E_T^{jet}$  dependence in the strong-coupling constant  $\alpha_s(\mu)$  ( $\mu \sim E_T^{jet}$ ).

In this paper, we study the  $E_T^{jet}$  dependence of the jet shape produced both in  $\gamma\gamma$  collisions and in  $e^+e^-$  annihilation process at the hadron level. The cone jet finding algorithm is applied for both reactions.

In the jet cone algorithm, so far, two kinds of jet shape variables, i.e. the jet profile function[13] and the jet width, have been used in experiments. The jet profile function is given by the fraction of the jet energy within an inner cone of a certain size. This has been used in  $p\bar{p}$  collisions at TEVATRON[17],  $\gamma p$  collisions by the ZEUS collaboration at HERA[18] and  $\gamma\gamma$ [8] and  $e^+e^-$ [19] collisions by the OPAL collaboration at LEP. On the other hand, the jet width was used for the first time in studies of  $\gamma p$  collisions by the H1 collaboration at HERA[20]. They applied the same method to the  $p\bar{p}$  data in UA1 and observed a scaling behavior of the jet width for the jets in  $\gamma p$  and  $p\bar{p}$  collisions[20].

We here extend the H1-method for the jets produced in  $\gamma\gamma$  collisions and  $e^+e^-$  annihilations. We measured the jet width as a function of  $E_T^{jet}$  for both inclusive-jet and dijet samples. The width was measured up to  $E_T^{jet} = 8$  GeV for  $\gamma\gamma$  collisions, which corresponds to 0.3 in  $x_T = \frac{2 \cdot E_T^{jet}}{\sqrt{s_{ee}}}$ . The region of  $x_T \sim 1$  could be measured by using  $e^+e^-$  annihilation events. The jet width for direct and resolved samples in  $\gamma\gamma$  collisions was also studied separately by reconstructing the momentum-fraction of the parton inside the photon for dijet events.

## 2 Experimental data

The data used in this analysis were taken with the TOPAZ detector at the TRISTAN  $e^+e^-$  collider (KEK) at an average center-of-mass energy of 58.0 GeV. All data taken for the period from 1990 to 1995 were used in this analysis, which corresponds to an integrated luminosity of 287.8 pb<sup>-1</sup>.

A detailed description of the TOPAZ detector can be found elsewhere [21]-[23]. In this analysis, both charged tracks and the neutral clusters were used for event selection and jet reconstruction. Charged tracks were measured in a 1.0 Tesla magnetic field with the time-projection-chamber (TPC) in the angular region of  $|\cos\theta| \leq 0.85$ , where  $\theta$  is the polar angle of a particle with respect to the beam axis. TPC provided a momentum resolution of  $\sigma_{p_t}/p_t = \sqrt{(1.5p_t)^2 + 1.6^2}$ (%), where  $p_t$  (in GeV) is the transverse momentum to the beam axis. Electromagnetic showers were detected with three kinds of calorimeters: a barrel lead-glass calorimeter (BCL), an end-cap Pb-proportional-wire-counter-sandwich calorimeter (ECL) and a forward bismuth-germanate-crystal calorimeter (FCL). Each detector covered polar angular ranges of  $|\cos\theta| \leq 0.85$ ,  $0.85 \leq |\cos\theta| \leq 0.98$  and  $0.972 \leq |\cos\theta| \leq 0.998$  ( $= 3.2^\circ$ ), respectively. Since FCL is located very close to the beam pipe, the calorimeter is protected from beam-induced backgrounds by an extensive shielding system [22].

In  $\gamma\gamma$  collisions, the detection efficiencies are sensitive to the trigger condition of charged tracks because of their low momentum and low multiplicity of tracks[23]. Through the experiments, the conditions of the charged track-trigger were changed according to the beam

conditions. There must be at least two tracks with  $p_t > 0.3 \text{ GeV} \sim 0.7 \text{ GeV}$ ; also the minimum opening angle of the two highest  $p_t$  tracks is  $45^\circ \sim 70^\circ$ . The change in the trigger conditions was taken into account in the TOPAZ simulation program. The effects on the jet width studied in this analysis were found to be negligible ( $< 1\%$ ).

### 3 Event selection and jet reconstruction

The hadronic events produced in  $\gamma\gamma$  collisions are selected in the following criteria:

1. The number of charged tracks with  $p_t > 0.1 \text{ GeV}$  and the polar angle  $|\cos\theta| < 0.83$  should be at least 4;
2. The position of the event vertex should be within 3.0 cm in the  $r\phi$ -plane and within  $\pm 3.0 \text{ cm}$  along the beam line from the interaction point;
3. The visible energy ( $E_{vis}$ ) of the event should satisfy  $E_{vis} \leq 35 \text{ GeV}$ , where both the charged tracks in TPC and the neutral clusters in BCL and ECL are used in the calculation of  $E_{vis}$ ;
4. The mass of the system of the observed hadrons ( $W_{vis}$ ) should be  $W_{vis} \geq 2 \text{ GeV}$ , where the tracks in TPC and the clusters in BCL and ECL are used; and
5. The energy of the most energetic cluster in BCL, ECL, or FCL should be less than  $0.25 \times E_{beam}$ .

These selection criteria leave 286k multihadron events. The criterion 5 ensures the anti-tag condition, which limits the scattering angle of the beam electrons to be less than  $3.2^\circ$ . With this anti-tag requirement, the virtuality ( $Q^2$ ) of the photons ranges from  $\sim 10^{-8} \text{ GeV}^2$  to  $2.6 \text{ GeV}^2$ . The mean value of  $Q^2$  is  $\sim 10^{-4} \text{ GeV}^2$ .

For the hadronic events in  $e^+e^-$  annihilation process, the standard cuts which have been used in the TOPAZ collaboration were applied to  $278.0 \text{ pb}^{-1}$  of data. The criteria used in the selection are described in ref.[24]. A total of 29k  $e^+e^-$  annihilation events were selected.

In order to identify jets in the hadronic events both in  $\gamma\gamma$  collisions and  $e^+e^-$  annihilation process, we used the conventional jet cone algorithm[25], where a jet is defined as a large amount of transverse energy (or momentum) concentrated in a cone of radius  $R$  in the  $\eta$ (pseudorapidity \*\*) -  $\phi$ (azimuthal angle) plane. A particle  $i$  is included in a jet if it lies within the cone

$$\sqrt{(\eta^{jet} - \eta^i)^2 + (\phi^{jet} - \phi^i)^2} \leq R. \quad (1)$$

In the cone algorithm, the transverse energy of the jet ( $E_T^{jet}$ ) is calculated as a scalar sum of the particle transverse energy ( $E_{t_i} = E_i \cdot \sin\theta_i$ ) in a cone,

$$E_T^{jet} = \sum_{i \in \text{cone}} E_{t_i}, \quad (2)$$

and the jet direction( $\eta^{jet}$  and  $\phi^{jet}$ ) is defined by the following weighted averages:

$$\eta^{jet} = \frac{1}{E_T^{jet}} \sum_{i \in \text{cone}} E_{t_i} \cdot \eta_i \quad \text{and} \quad \phi^{jet} = \frac{1}{E_T^{jet}} \sum_{i \in \text{cone}} E_{t_i} \cdot \phi_i. \quad (3)$$

---

\*\*Pseudorapidity  $\eta$  is defined in terms of the polar angle  $\theta$  as  $\eta \equiv -\ln \tan(\theta/2)$ . The electron-beam direction is taken to be the + z direction in this experiment.

The jet direction is determined by iteration. The iteration is stopped when particles contained in the cone are not changed in the next iteration.

When two or more jets overlap each other, particles in the overlapped region were assigned to the highest  $E_T^{jet}$  jet in this analysis <sup>††</sup>. In jet reconstruction, all charged particles with a transverse momentum greater than 0.10 GeV and neutral particles with an energy greater than 0.3 GeV were used. In this analysis, the size of the cone radius( $R$ ) was fixed at  $R = 1.0$ .

The detector effects on the jet  $E_T^{jet}$  and jet directions ( $\eta^{jet}, \phi^{jet}$ ) were checked by using Monte-Carlo samples generated by the PYTHIA program (version: 5.720)[26]. The results show that the jet directions( $\eta^{jet}, \phi^{jet}$ ) have good correlations between the generated and observed quantities. The resolutions are  $\sigma_{\eta^{jet}} = 0.05$  and  $\sigma_{\phi^{jet}} = 0.06$  for  $\eta^{jet}$  and  $\phi^{jet}$ , respectively. However,  $E_T^{jet}$  in the observed level is systematically lower than the generated (hadron level) one by about 13%. This effect has been corrected in the data. After correcting  $E_T^{jet}$ , 39,829 inclusive-jets in  $\gamma\gamma$  collisions are selected with the conditions of  $E_T^{jet} \geq 2.0$  GeV and  $|\eta^{jet}| \leq 0.7$ . Dijet events are selected by taking an event with two or more jets with fulfilling that the highest  $E_T^{jet}$  be greater than 3.0 GeV and the second highest  $E_T^{jet}$  be greater than 2.0 GeV[27]. The pseudorapidity of both jets is required to be within  $|\eta^{jet}| \leq 0.7$ . With this condition, 3,582 dijet events are selected.

The beam-gas background remaining in the inclusive-jet and dijet samples was estimated to be 11.2% and 0.70%, respectively, from the number of events in the side-band of the event-vertex distribution along the beam-axis. The physical background mainly comes from  $e^+e^-$  annihilation events:  $e^+e^- \rightarrow q\bar{q}(\gamma)$ . The contribution of this background has been estimated from the KORALZ[28] and PYTHIA programs to be 9.54% and 18.4% for inclusive-jet and dijet samples, respectively. The other physical backgrounds ( $e^+e^- \rightarrow \tau^+\tau^-(\gamma)$ ,  $e^+e^- \rightarrow e^+e^-\tau^+\tau^-$  and  $e^+e^- \rightarrow e^+e^-e^+e^-$ ) were found to be 0.19% (0.61%), 1.21% (2.48%) and 0.28% (0.86%) for the inclusive-jet (dijet) samples. Hereafter, these backgrounds are subtracted from data on a bin-by-bin basis.

## 4 Direct and resolved contributions in dijet events

We first demonstrate how the direct and resolved contributions can be separated in the dijet sample in  $\gamma\gamma$  collisions. This separation is a useful tool to study the jet width from direct and resolved processes independently. Other detailed studies of the hadronic final state in this dijet sample are given in ref.[9].

In the leading-order QCD, two hard partons are produced in  $\gamma\gamma$  collisions. In the one- or two-resolved processes, two high- $E_T^{jet}$  jets are expected to be accompanied by one or two remnant jets in the near beam-direction[4]. A pair of variables,  $x_\gamma^+$  and  $x_\gamma^-$  can then be

---

<sup>††</sup>This point is different from our previous analysis[1], where two jets are combined if their directions satisfy the condition recommended by Ellis *et al.* in ref.[25]. However, we do not use this method in this analysis, because when there are more than three seed-jets, they are sometimes recombined into one jet, and the size of the jet cone becomes very big by the iteration of the recombination. This mainly happens when there are activities from remnant-jets in an event.

defined which specify the fraction of the photon momentum carried by the parton inside the photon in hard interactions. One can calculate  $x_\gamma^\pm$  from the observables with a good approximation [5]:

$$x_\gamma^+ = \frac{\sum_{j \in \text{jets}} (E - p_z)_j}{\sum_{i \in \text{hadrons}} (E - p_z)_i} \quad \text{and} \quad x_\gamma^- = \frac{\sum_{j \in \text{jets}} (E + p_z)_j}{\sum_{i \in \text{hadrons}} (E + p_z)_i}, \quad (4)$$

where  $p_z$  is the momentum component along the  $z$ -axis of the detector and  $E$  is the energy of each particle or jet. The numerator of Eq.(4) is the sum for particles within the jet cone, while the denominator is the sum for all particles in a dijet event. Since the direction of the electron beam is taken to be the positive direction of the  $z$ -axis in the TOPAZ convention,  $x^-$  ( $x^+$ ) corresponds to the parton-momentum fraction of the photon radiated from electron (positron) beam. We introduce a variable,  $x_\gamma^{\text{min}}$ , which is defined as the smaller value of  $x_\gamma^-$  and  $x_\gamma^+$ .

In Fig.2, the distribution of  $x_\gamma^{\text{min}}$  is compared with the Monte-Carlo predictions of the PYTHIA (5.720) program, where no correction for the selection cut and the detector effects has been applied, but the background has been subtracted. The contribution from the direct and resolved processes, predicted by PYTHIA, are also shown separately. The predictions of PYTHIA are normalized to the luminosity of data by taking into account the predicted cross sections. The clear peak seen in the vicinity of  $x_\gamma^{\text{min}} \sim 1$  can be well-explained from the direct component. In the low- $x_\gamma^{\text{min}}$  region ( $x_\gamma^{\text{min}} \leq 0.8$ ), where the contribution from the resolved processes dominates, it is found that the overall shape as well as its magnitude are well explained by PYTHIA with the GRV-LO photon structure function[29], though for the region around  $0.2 \leq x_\gamma^{\text{min}} \leq 0.6$  the prediction is about 20% higher than the data. (The comparison with other cases are given in ref.[9]).

In an analysis of the jet width, the direct and resolved samples are separated at  $x_\gamma^{\text{min}} = 0.85$ . In the Monte-Carlo simulation of PYTHIA, about 67% of the events from the direct process are contained in the  $x_\gamma^{\text{min}} > 0.85$  region, while about 90% of the events from the resolved process are contained in the  $x_\gamma^{\text{min}} < 0.85$  region.

## 5 Transverse energy flow and jet width

The transverse energy flow versus the azimuthal angle around the jet direction is shown in Fig.3a for inclusive-jets with  $3.0 < E_T^{\text{jet}} < 4.0$  GeV and  $|\eta^{\text{jet}}| < 0.7$  in  $\gamma\gamma$  collisions. In a plot the pseudo-rapidity of each particle is limited to within 1.0 unit in order to avoid any effect from the remnant-jets. Fig.3b shows the same transverse energy flow for  $e^+e^-$  annihilation events with the same jet cone algorithm. The value of  $E_T^{\text{jet}}$  is required to be greater than 15 GeV. Although both energy flows in  $\gamma\gamma$  and  $e^+e^-$  collisions show a similar jet profile, the width is very different.

In order to make the discussion more quantitative, we define the jet width as the full width at the half maximum of the distribution of the transverse energy flow ( $\frac{1}{N} \frac{dE_T}{d\phi}$ ). This

jet width is determined by fitting the energy flow with the following formula:

$$f(\Delta\phi) = A \cdot \exp\{-\sqrt{|\Delta\phi| + B}^4 + B^4\} + C, \quad (5)$$

where  $\Delta\phi$  is the azimuthal angle difference between the jet direction and each particle. Parameter  $A$  describes the amplitude of the energy flow at  $\Delta\phi = 0$ , and  $C$  reflects the constant pedestal energy below the peak. The jet width ( $\Gamma$ ) can be obtained from the parameter  $B$  as

$$\Gamma = 2\{(\ln 2 + B^4)^{1/4} - B\}^2.$$

This is the same formula as that used in the H1 experiment for the analysis of the jet width in  $\gamma p$  reactions [20]. The fit is carried out only in the peak region,  $|\Delta\phi| < 1.5$ .

Since the jet width can be measured by using only a fiducial volume of the detector, it is expected that the distortion caused by the detector is small, but not negligible. A finite detection efficiency of the charged and neutral particles as well as their finite resolutions might distort the original jet width. We correct these detector effects by Monte-Carlo simulations. The jet width in the hadron level ( $\Gamma^{cor}$ ) is obtained in each  $E_T^{jet}$  bin from the formula

$$\Gamma^{cor} = \Gamma^{obs} \times \frac{1}{\Gamma_{MC}^{obs}/\Gamma_{MC}^{hadron}}, \quad (6)$$

where  $\Gamma^{obs}$  is the width measured in data;  $\Gamma_{MC}^{obs}$  and  $\Gamma_{MC}^{hadron}$  are the width at the observed and the generator (hadron) level in the Monte-Carlo simulation, respectively. The PYTHIA and PHOJET[30] programs are used to determine the correction factor ( $\Gamma_{MC}^{obs}/\Gamma_{MC}^{hadron}$ ). The correction factors ranges from -15% to +15%, depending on the  $E_T^{jet}$  region. The bin-size of  $E_T^{jet}$  is determined from the consideration of the detector resolution of  $E_T^{jet}$ .

## 6 Results and Discussions

The results on the jet width ( $\Gamma$ ) for jets produced in  $\gamma\gamma$  collisions and for  $e^+e^-$  annihilation process are summarized in Table 1. In this table, the first errors are statistical and the second ones are systematics. The systematic errors on the width are estimated by changing the size of the  $\Delta\phi$  bin by factors from 1/5 to 5 to the nominal bin-size shown in Fig.3. The systematics caused by these binning effects are estimated to be less than 3%. The systematics estimated from the difference of the correction factors in PYTHIA and PHOJET programs are about  $\pm 2\%$ . In the fit, a pedestal energy below the peak is assumed to be constant in Eq.(5). The systematics by adding a linear term are negligible ( $\leq 0.1\%$ ).

In Fig.4a, the corrected jet widths ( $\Gamma$ ) in  $\gamma\gamma$  interactions as well as the  $e^+e^-$  annihilation events are shown as a function of  $E_T^{jet}$ . The solid circles are the width from the inclusive-jets and solid triangles are that from dijet sample. The solid squares are the jet width for the  $e^+e^-$  annihilation events. Since the sample of the inclusive-jets and dijet events are almost identical in the  $e^+e^-$  annihilation events, only the results from the inclusive-jets are plotted. In this figure, the errors include statistical and systematic errors added in quadrature. In the same figure, the results in  $\gamma p$  collisions from H1 experiment at HERA[20] and  $p\bar{p}$  at UA1



experiment[31] are also shown for a comparison. The following points can be observed from Fig.4a:

1. In the  $E_T^{jet}$  region below 4 GeV, the jet width ( $\Gamma$ ) in  $\gamma\gamma$  collisions is almost constant.
2. Above  $E_T^{jet} > 4$  GeV, the width of jets in  $\gamma\gamma$  decreases as their  $E_T^{jet}$  increases.
3. The jet width in  $e^+e^-$  annihilation events located, approximately, at the extrapolated points linearly on the  $E_T^{jet}$  dependence in  $\gamma\gamma$  collisions.
4. At the same value of  $E_T^{jet}$ ,  $E_T^{jet} = 8$  GeV for example, the jet width in  $\gamma\gamma$  collisions at TRISTAN is 3.5-times narrower than that measured in  $\gamma p$  collisions at HERA.
5. The width in  $p\bar{p}$  data from UA1 experiment is much wider than that in  $\gamma p$  collisions at HERA and also  $\gamma\gamma$  collisions at TRISTAN at the same value of  $E_T^{jet}$ .

It should be emphasized that the wide dynamic range of  $E_T^{jet}$  from 2 GeV to several 10 GeV is covered in Fig.4a.

According to the suggestions of the QCD analysis of jet shapes in refs.[14, 15], the widths of jets from  $\gamma\gamma$ ,  $\gamma p$ ,  $p\bar{p}$  interactions are plotted as a function of the scaled transverse energy  $x_T \equiv 2E_T^{jet}/\sqrt{s}$  in Fig.4b. Although there are no discussion about  $e^+e^-$  annihilation events in refs.[14, 15], the jet width in  $e^+e^-$  events are also plotted as a function of  $x_T$  in the same figure. In the definition of  $x_T$ ,  $\sqrt{s}$  represents the center-of-mass (cms) energy of initial beam particles in collisions. The cms energy of the  $e^+e^-$  system ( $\sqrt{s_{ee}} = 58$  GeV) is taken for  $\gamma\gamma$  interactions at TRISTAN<sup>‡‡</sup>, the  $ep$  cms energy ( $\sqrt{s_{ep}} = 297$  GeV) is taken for  $\gamma p$  interactions at HERA (H1) and  $\sqrt{s_{p\bar{p}}} = 540$  GeV and 630 GeV is taken for UA1  $p\bar{p}$  data. The  $\gamma p$  data at HERA covers 0.02 - 0.1 in  $x_T$ , while the  $\gamma\gamma$  data at TRISTAN covers relatively high- $x_T$  regions of 0.08 - 0.3. Two points are plotted for the  $e^+e^-$  annihilation events. The lower point at  $x_T = 0.42$  corresponds to the radiative events ( $e^+e^- \rightarrow q\bar{q}\gamma$ ).

One can observe from Fig.4b that the jet width in different reactions and the different energies are approximately compatible with having the same dependence on the scaled transverse jet energy  $x_T$ . It is discussed in refs.[14, 15] that this kind of scaling behavior is in fact expected from perturbative-QCD for the jet shape in hadron-hadron and (resolved) $\gamma p$  and  $\gamma\gamma$  collisions. Although the scaling violation is expected through the  $E_T^{jet}$  dependence in the strong-coupling constant ( $\alpha_s$ ), this point is not clear from these data alone. It is also not clear in this moment that this kind of argument can be extended to the  $e^+e^-$  annihilation processes[32].

In order to check the possible difference of the jet width in direct and resolved processes in  $\gamma\gamma$  collisions, the jet width in dijet events was studied. Fig.5a shows the jet width for a direct-enriched ( $x_\gamma^{min} > 0.85$ ) and a resolved-enriched ( $x_\gamma^{min} < 0.85$ ) sample. The results

---

<sup>‡‡</sup> The reason why  $\sqrt{s_{ee}}$  should be taken instead of  $\sqrt{s_{\gamma\gamma}}$  is caused by the continuous energy spectrum of the photons. In the jet cross sections or the jet shape we observe, the photon energy spectrum is integrated over the full kinematical regions. As a result, the dependence of  $\sqrt{s_{\gamma\gamma}}$  disappears and only that of  $\sqrt{s_{ee}}$  remains.

show that the jet width in the direct sample (solid circles) is narrower than that of the resolved sample (solid squares) by about 0.05 radian in the region from  $E_T^{jet} = 4$  to 7 GeV. Above  $E_T^{jet} > 7$  GeV the statistical errors become big. Since jets originate only from quarks in the direct process and jets originate from gluons are included in the resolved processes, this difference might be caused by the shape difference of quark- and gluon-jets, though the difference is within twice the standard deviation.

In Fig.5b the jet width in  $\gamma\gamma$  collisions and in  $e^+e^-$  annihilation events is compared with PYTHIA predictions. The solid line is the prediction with the default parameters of the program where both initial and final parton showers are included. The dotted line is the one with turning off the parton showers. For the hadronization parameters in the program, the default values which have been determined by  $e^+e^-$  annihilation events at LEP1[5] are used.

Fig.5b indicates that in the region above 3 GeV the perturbative parton shower plays an important role concerning the jet width. The PYTHIA reproduces the measured jet width in  $\gamma\gamma$  interactions as well as  $e^+e^-$  annihilation events quite well.

## 7 Conclusion

We have studied the width of the jets produced in  $\gamma\gamma$  collisions as well as  $e^+e^-$  annihilation process with the jet cone algorithm. The jet width in  $\gamma\gamma$  collisions becomes narrower as their  $E_T^{jet}$  increases above 4 GeV. The jet width in  $e^+e^-$  annihilation events is found to be located at the linearly extrapolated points from the  $E_T^{jet}$  dependence in  $\gamma\gamma$  collisions. Even at the same  $E_T^{jet}$ , a large difference in the jet width has been observed in jets in  $\gamma\gamma$  at TRISTAN,  $\gamma p$  at HERA and  $p\bar{p}$  at the UA1 experiment. An approximate scaling behavior of the jet width in the different reaction and the different energy is observed if the width is plotted as a function of  $x_T$ .

This observation might be important for a comparison of the jet shape in different reactions. In ref.[19] the shape difference of the quark and gluon are discussed by comparing the shape of the jets in similar  $E_T^{jet}$  regions produced in  $e^+e^-$  and  $p\bar{p}$ [17] collisions. However, the result of our analysis suggests that the jet shape in the different reactions should be compared at the same  $x_T$  region.

## Acknowledgment

We appreciate useful discussions with Drs. D. Aurenche, M. Drees, K. Kramer concerning this analysis. We thank the TRISTAN accelerator staff for the successful operation of TRISTAN. We also thank all of the engineers and technicians at KEK and the other collaborating institutions: Messrs H. Inoue, N. Kimura, K. Shiino, M. Tanaka, K. Tsukada, N. Ujiie, and H. Yamaoka.

## References

- [1] TOPAZ Collab., H. Hayashii *et al.*, Phys. Lett. **B314** (1993) 149;  
Proc. on 10th workshop on  $\gamma\gamma$  collisions and related process, Sheffield,(World Scientific, Apr. 1995) 133.
- [2] AMY Collab., B. J. Kim *et al.*, Phys. Lett. **B325** (1994) 248;  
AMY Collab., R. Tanaka *et al.*, Phys. Lett. **B277** (1992) 215.
- [3] ALEPH Collab., D. Buskulic *et al.*, Phys. Lett. **B313** (1993) 509;  
DELPHI Collab., P. Abreu *et al.*, Z. Phys. **C62** (1994) 357.
- [4] see e.g., M. Drees and R. M. Godbole, Nucl. Phys. **B339** (1990) 355;  
M. Erdmann, Springer Tracts in Modern Physics **138** (1997);  
G. A. Schuler and T. Sjöstrand, Nucl. Phys. **B407** (1993) 539.
- [5] L. Lönnblad and M. Seymour (conveners),  $\gamma\gamma$  Event Generators, in “Physics at LEP2”,  
CERN 96-01, Vol.2 (1996) 187.
- [6] P. Aurenche, J.-Ph. Guillet *et al.*, Prog. Theo. Phys. **92** (1994) 175.
- [7] T. Kleinwort, G. Kramer, Phys. Lett. **B370**(1996)141;  
M. Klasen, T. Kleinwort and G. Kramer, Eur. Phys. J. direct **C1** (1998) 1.
- [8] OPAL Collab., K. Ackerstaff *et al.*, Z. Phys. **C73** (1997) 433;  
OPAL Collab., G. Abbiendi *et al.*, CERN preprint CERN-EP/98-113 and hep-ex/9808027 (1998).
- [9] TOPAZ Collab., H. Hayashii, Proc. on the workshop on photon interactions and the  
photon structure, Lund, September 10-13,1998.
- [10] TOPAZ Collab., M. Iwasaki *et al.*, Phys. Lett. **B341** (1994) 99;  
TOPAZ Collab., R. Enomoto *et al.*, Phys. Rev. **D50** (1994) 1879.
- [11] ZEUS Collab., M. Derrick *et al.*, Phys. Lett. **B384** (1996) 401;  
ZEUS Collab., J. Breitweg *et al.*, Eur. Phys. J. **C1** (1998) 109.
- [12] H1 Collab., T. Ahmed *et al.*, Nucl. Phys. **B445** (1995) 195;  
H1 Collab., C. Adloff *et al.*, Eur. Phys. J. **C1** (1998) 97.
- [13] S. D. Ellis, Z. Kunszt and D. E. Soper, Phys. Rev. Lett. **69** (1992) 3615.
- [14] G. Kramer, S. G. Salesch, Phys. Lett. **B333** (1994) 519.
- [15] M. Klasen, G. Kramer, Phys. Rev. **D56** (1997) 2702.
- [16] M. H. Seymour, Nucl. Phys. **B513** (1998) 269, hep-ph/9707338 (1997).
- [17] CDF Collab., F. Abe *et al.*, Phys. Rev. Lett. **70** (1993) 713;  
D0 Collab., S. Abachi *et al.*, Phys. Lett. **B357** (1995) 500.

- [18] ZEUS Collab. J. Breitweg *et al.*, Eur. Phys. J. **C2** (1998) 61.
- [19] OPAL Collab., R. Akers *et al.*, Zeit. Phys. **C63** (1994) 197.
- [20] H1 Collab., S. Aid *et al.*, Z. Phys. **C70** (1996) 17.
- [21] T. Kamae *et al.*, Nucl. Inst. and Meth. **A252** (1986) 423;  
 S. Kawabata *et al.*, Nucl. Inst. and Meth. **A270** (1988) 11;  
 K. Fujii *et al.*, Nucl. Inst. and Meth. **A236** (1985) 55;  
 J. Fujimoto, *et al.*, Nucl. Inst. and Meth. **A256** (1987) 449;  
 H. Hayashii *et al.*, Nucl. Inst. and Meth. **A316** (1992) 202.
- [22] H. Kichimi *et al.*, Nucl. Inst. and Meth. **A334** (1993) 367.
- [23] R. Enomoto *et al.*, Nucl. Inst. and Meth. **A269** (1988) 507;  
 T. Tsukamoto, M. Yamauchi and R. Enomoto, Nucl. Inst. and Meth. **A297** (1990) 148.
- [24] TOPAZ Collab., K. Nakabayashi *et al.*, Phys. Lett. **B413** (1997) 447.
- [25] S. Ellis, Z. Kunszt, D. E. Soper, Phys. Rev. **D40** (1989) 2188.
- [26] T. Sjöstrand, Comp. Phys. Comm. **82** (1994) 74;  
 T. Sjöstrand, Lund University report LU TP 95-20 (1995).
- [27] S. Frixione, G. Ridolfi, Nucl. Phys. **B507** (1997) 315.
- [28] S. Jadach, B.F.L. Ward and Z. Was, Comm. Phys. Comm. **66** (1991) 276.
- [29] M. Glück, E. Reya, A. Vogt, Phys. Rev. **D46** (1992) 1973.
- [30] R. Engel and J. Ranft, Phys. Rev. **D54** (1996) 4244;  
 R. Engel, Z. Phys. **C66** (1995) 203;  
 R. Engel, University Siegen preprint 95-05.
- [31] UA1 Collab., C. Albajar *et al.*, Nucl. Phys. **B309** (1988) 405;  
 UA1 Collab., G. Arnison *et al.*, Phys. Lett. **B132** (1983) 214.
- [32] G. Kramer, private communication.

## Table caption

Reaction	$E_T^{jet}$ (GeV)	$\langle E_T^{jet} \rangle$ (GeV)	Jet Width ( $\Gamma$ )	
			inclusive-jet	dijet
$\gamma\gamma$ coll.	2.0 - 3.0	2.37	$0.394 \pm 0.006 \pm 0.016$	
	3.0 - 4.0	3.40	$0.415 \pm 0.010 \pm 0.017$	$0.349 \pm 0.012 \pm 0.015$
	4.0 - 5.5	4.59	$0.391 \pm 0.012 \pm 0.016$	$0.348 \pm 0.014 \pm 0.015$
	5.5 - 7.5	6.30	$0.327 \pm 0.018 \pm 0.014$	$0.336 \pm 0.020 \pm 0.014$
	7.5 - 9.5	8.34	$0.217 \pm 0.026 \pm 0.009$	$0.192 \pm 0.021 \pm 0.008$
$e^+e^-$ annih.	10 - 15	13.0	$0.153 \pm 0.003 \pm 0.006$	$0.154 \pm 0.007 \pm 0.006$
	15 - 40	22.9	$0.091 \pm 0.001 \pm 0.004$	$0.087 \pm 0.001 \pm 0.004$

Table 1: Jet width ( $\Gamma$ ) in  $\gamma\gamma$  collisions and  $e^+e^-$  annihilation events as a function of  $E_T^{jet}$  for jets in the central region  $|\eta^{jet}| < 0.7$ .  $\langle E_T^{jet} \rangle$  is the averaged  $E_T^{jet}$  weighted by the number of events in each  $E_T^{jet}$  bin. The maximum value of  $E_T^{jet}$  is taken for a dijet sample. The first error is statistical and the second error is systematic.

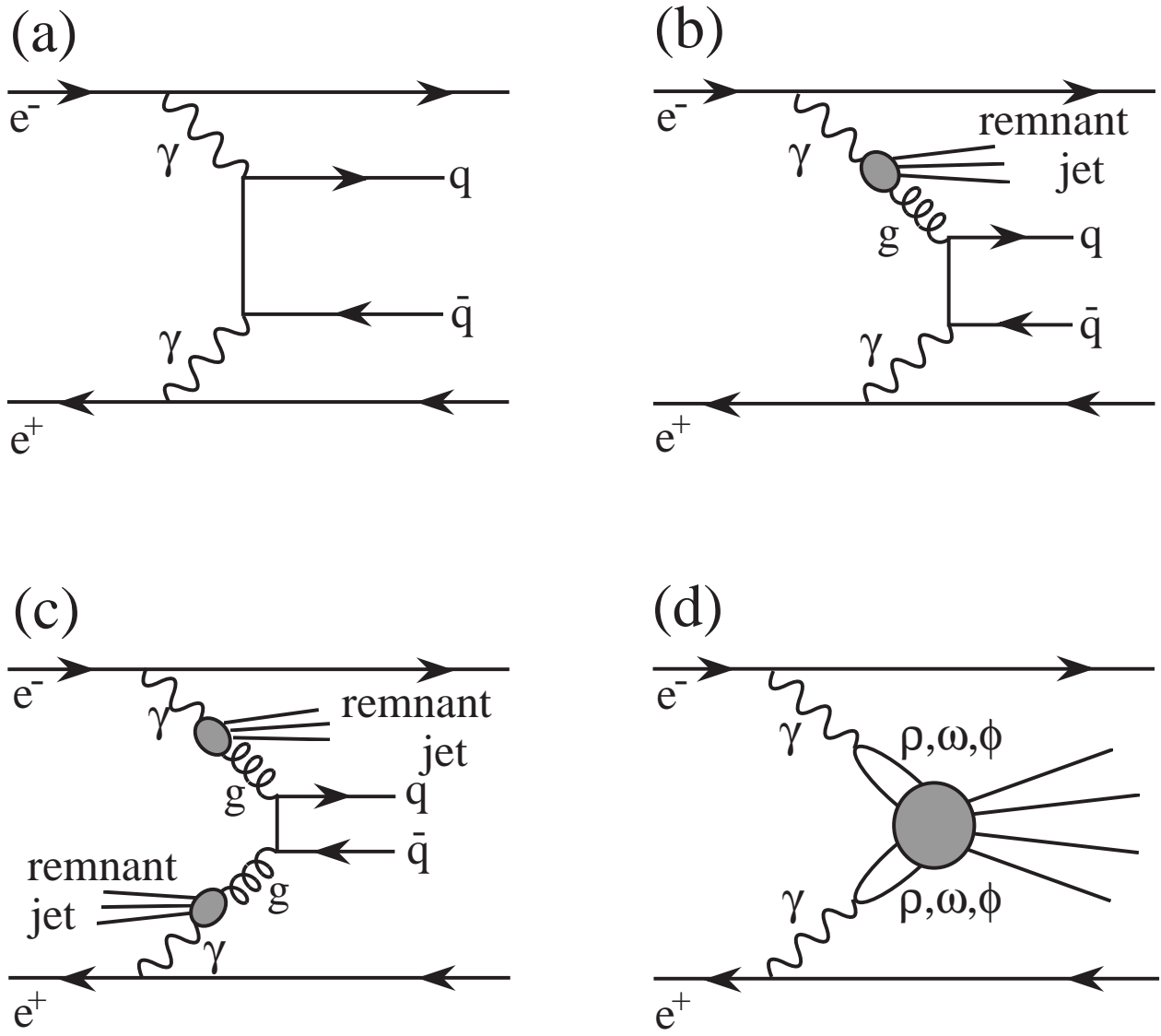


Figure 1: Examples of diagrams contributing to the hadron production in  $\gamma\gamma$  collisions: (a) direct(QPM) process, (b) one-resolved process, (c) two-resolved process and (d) soft VDM process.

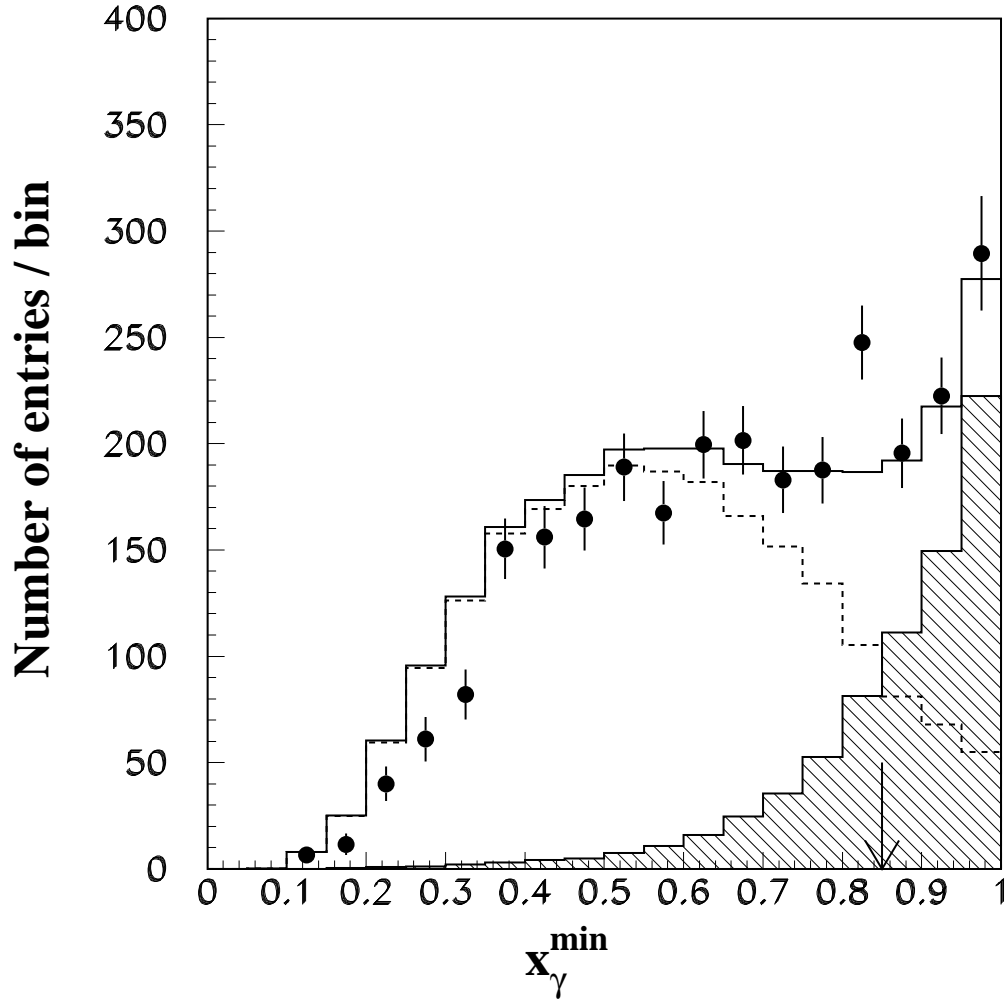


Figure 2:  $x_{\gamma}^{\min}$  distribution for dijet events in  $\gamma\gamma$  collisions. Data (solid circles) are compared to the predictions of PYTHIA, where the GRV-LO photon structure function with  $p_t^{\min}=1.6$  GeV is used. The hatched histogram is the contribution from the direct process, and the dashed one is that from the resolved processes. The solid one is the sum of both processes. The arrow at  $x_{\gamma}^{\min} = 0.85$  indicates the division between direct ( $> 0.85$ ) and resolved ( $< 0.85$ ) events. Only statistical errors are shown. The Monte-Carlo predictions are normalized to the data luminosity by taking into account the predicted cross sections.

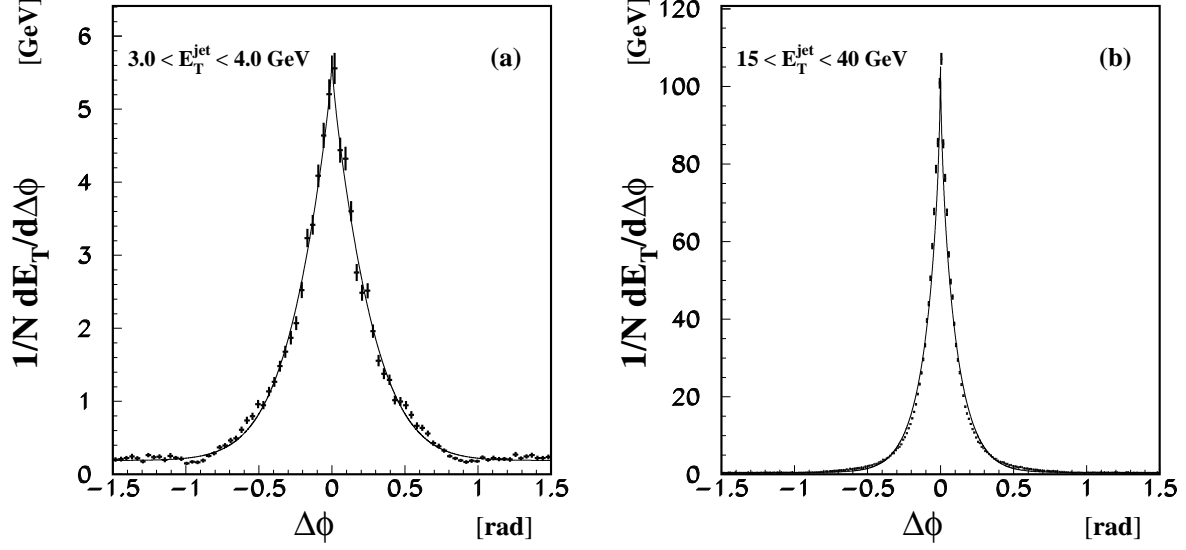


Figure 3: Transverse energy flows with respect to the jet direction projected into the azimuthal direction ( $\Delta\phi$ ): (a) for the inclusive-jets in  $\gamma\gamma$  collisions with  $3.0 < E_T^{jet} < 4.0$  GeV and  $|\eta^{jet}| < 0.7$ ; (b) for the inclusive-jets in  $e^+e^-$  annihilation events with  $E_T^{jet} > 15$  GeV. Solid line in each figure is the result of a fit with a formula given in Eq.(5).



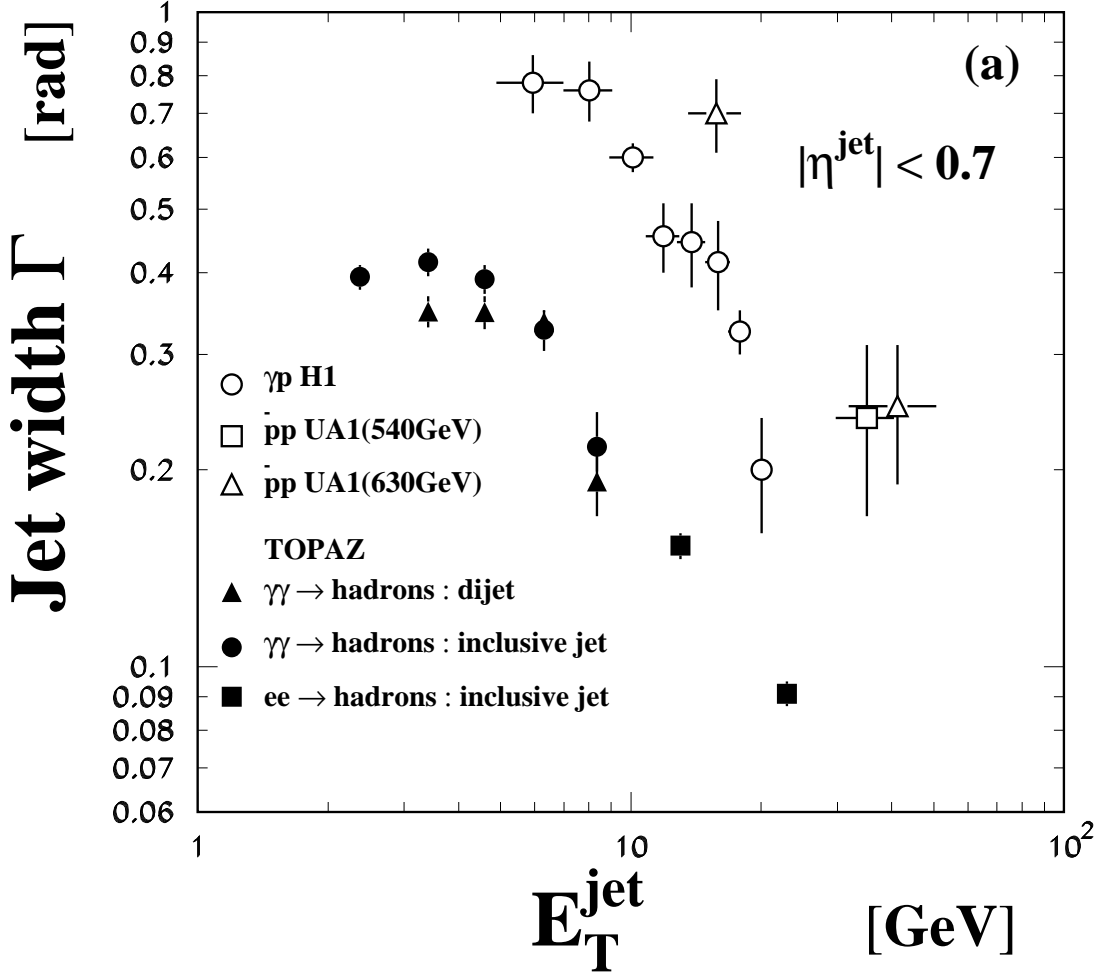


Figure 4: (a) Jet width as a function of  $E_T^{\text{jet}}$  for the inclusive-jets (solid circles) and dijet (solid triangles) in  $\gamma\gamma$  collisions as well as for the inclusive-jets (solid squares) in  $e^+e^-$  annihilation process at  $\sqrt{s_{e^+e^-}} = 58$  GeV. The maximum value of  $E_T^{\text{jet}}$  is taken for the dijet sample. The error bar shows the statistical error and the systematic error added in quadrature. For a comparison, the jet widths in other reactions are also plotted. The open circles show the jet width in  $\gamma p$  collisions at  $\sqrt{s_{ep}} = 540$  GeV[20]. The open square and open triangles show the width in  $p\bar{p}$  collisions at  $\sqrt{s} = 540$  GeV and  $\sqrt{s} = 630$  GeV, respectively[31].

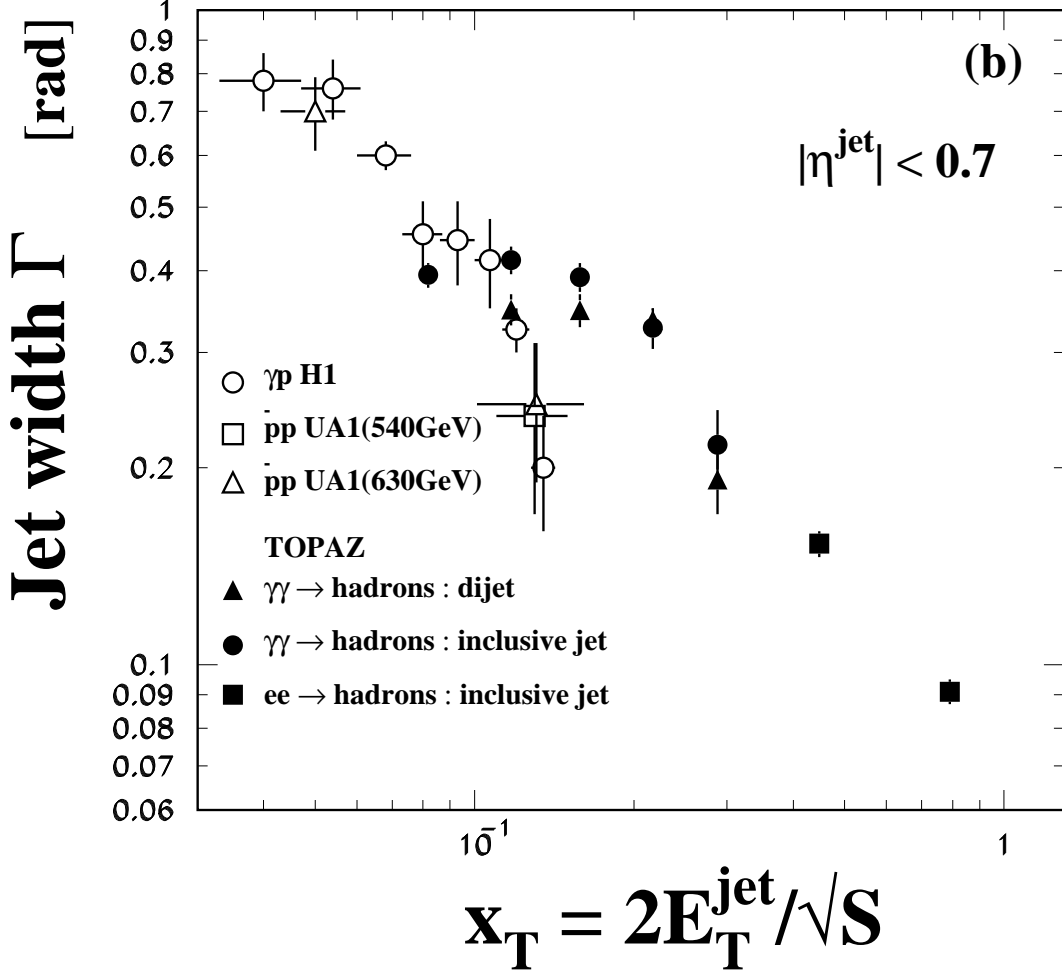


Figure 4: (b) Jet width as a function of  $x_T \equiv 2E_T^{\text{jet}}/\sqrt{s}$ , where  $\sqrt{s}$  represents the center-of-mass energy of the initial beam system. The meaning of the symbols is given in Fig.4a. The error bars show the statistical and systematic errors added in quadrature.

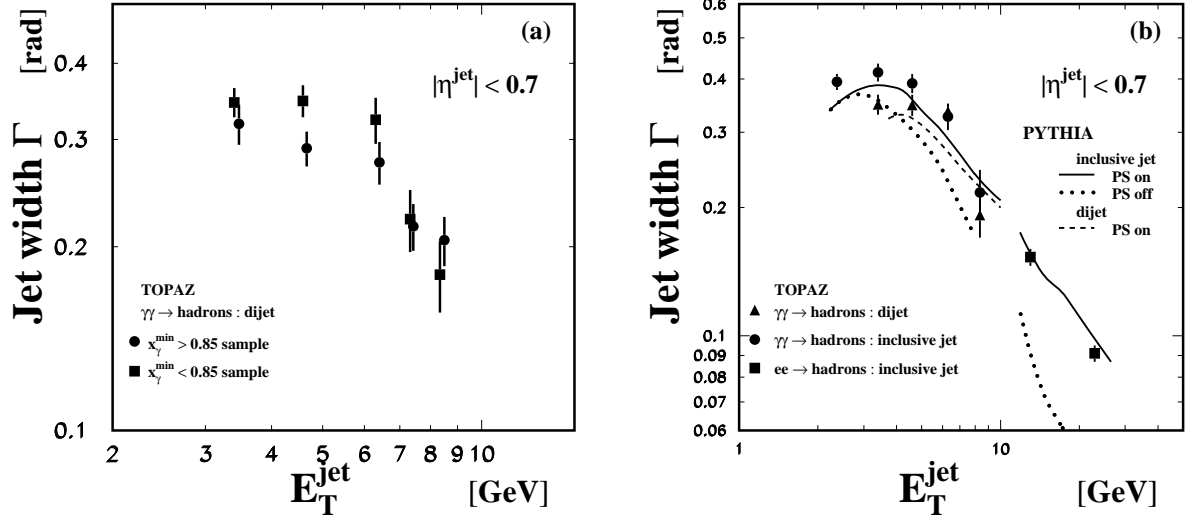


Figure 5: (a) Comparison of the jet width in direct and resolved samples. The solid circles are results for a direct sample ( $x_\gamma^{\text{min}} > 0.85$ ), and the solid squares for a resolved sample ( $x_\gamma < 0.85$ ). The error bars show the statistical and systematic errors added in quadrature. (b) Comparison of the jet width with PYTHIA Monte-Carlo predictions with the parton shower (solid line) and without parton shower (dotted line). The dashed line shows the Monte-Carlo predictions for a dijet sample.